

Can the Calcined Weathered Stones be Employed as Anode Materials for Lithium Ion Batteries?

Keqiang Ding^{1,*}, Binjuan Wei¹, Yan Zhang¹, Chenxue Li¹, Xiaomi Shi¹ and Junqing Pan^{2,†}

¹College of Chemistry and Materials Science, Hebei Normal University, Shijiazhuang, Hebei 050024, P.R. China

²State Key Laboratory of Chemical Resource Engineering, Beijing University of Chemical Technology, Beijing, 100029, China

Received: August 23, 2017, Accepted: October 23, 2017, Available online: November 02, 2017

Abstract: A novel finding, that the calcined weathered stones (denoted as CWS) can be employed as the anode materials for lithium ion batteries (LIBs), is reported for the first time in this work. Under the air conditions, the weathered stones were respectively calcined at 400°C (sample a), 600°C (sample b) and 800°C (sample c) for 2 h, with an intention to examine the influence of the calcination temperature on the physicochemical properties of the resultant materials. XRD results indicated that the main components of all the final products were SiO₂. And the SEM images demonstrated that all the as-prepared samples were irregular and larger particles with no evident crystal structure. The results of the electrochemical measurements revealed that the initial discharge capacity of sample b was about 104 mAh g⁻¹ at the current density of 100 mA g⁻¹, which was remarkably larger than that of the employed pure SiO₂ (50 mAh g⁻¹). Interestingly, after 20 cycles, the discharge capacity of sample b was still maintained as high as 70 mAh g⁻¹, along with a capacity retention rate of about 70%. Although the discharge capacity reported here was lower as compared to the currently reported anode materials, this novel finding was very meaningful to the large scale production of anode materials, mainly due to the rather lower cost and abundant resources as well as the simple preparation process.

Keywords: weathered stone; calcination; calcination temperature; anode materials; lithium ions battery

1. INTRODUCTION

The main purpose of this pioneering work is to show the fact that the calcined weather stones can be used as anode materials for LIBs.

As we know, a lithium-ion battery is generally constructed by four parts, i.e., anode, cathode, electrolyte and separator, and among these four parts, both anode and cathode materials are the crucial factors which can directly determine both the capacity value and the service life of a lithium-ion battery [1]. Along with the research works concerning cathode materials, the anode materials have also been extensively investigated mainly due to the following reasons [2]. (1) The theoretical capacity (372 mAh g⁻¹) of graphite is particularly lower which cannot meet the demand of high power and high energy density of LIBs, though graphite as a conventional anode material has been commercialized in LIBs for years [3]. (2) The appearance of Li dendrites on the surface of graphite is unavoidable which may lead to the safety issue such as

short circuit and fire accidents particularly when being overcharged [4]. (3) A kind of so-called solid electrolyte interphase (SEI) layer will form on the surface of graphite due to the reduction reaction of the electrolyte, which is commonly detrimental to the electrochemical performance of a lithium ion battery especially in terms of the capacity and the cycle-life [5]. Therefore, many new kinds of anode materials were developed recently, desiring to replace the present anode material of graphite while maintaining a better electrochemical performance relative to that of graphite.

Summarily, till present, there are four kinds of novel anode materials, namely, new types of carbon such as graphene [6] and carbon nanodots [7], elementary substance such as Si [8] and Sn [9], metal oxides like SnO₂ [10], Co₃O₄ [11] and NiO [12], and lithium ions-contained metal oxides such as lithium titanate (Li₄Ti₅O₁₂) [13,14], though some other novel anode materials like Fe₂O₄-based materials [15] were also prepared in last several years. Although, as mentioned above, many novel kinds of anode materials have been developed, the practical applications of these so-called newly developed anode materials are very rare. To our knowledge, the relatively higher preparation cost and the poor

To whom correspondence should be addressed:

*Email: dkeqiang@263.net, Tel:+86-311-80787400; Fax:+86-311-80787401

†Email: jqpan@mail.buct.edu.cn, Tel:+86-10-64449332; fax:+86-10-64449332

electrochemical performance were the main factors which had badly hampered the further commercialization of these novel anode materials. For example, the pulverization of Si and Sn anode materials, which was mainly caused by the large volume change during cycling, was regarded as the major reason impeding their further commercialization [8, 9]. The rather lower electrical conductivity, as reported, should be responsible for the poor electrochemical performance of metal oxides-based anode materials [16]. Thus, developing novel anode materials is still an urgent topic especially for the LIBs-related researchers [17]. To the best of our knowledge, this is the first time to report that the sintered weathered stones can be employed as anode materials for LIBs.

In the present work, anode materials were prepared from weathered stones directly by using an air condition calcination method. The influence of calcination temperature on the physicochemical properties of synthesized materials was thoroughly examined, showing that as the calcination temperature was 600 °C (sample b), the best electrochemical behavior was exhibited by the synthesized sample. It was found that the discharge capacity of sample b was close to 70 mAh g⁻¹ after 20 cycles at the current density of 100 mA g⁻¹. It is true that the electrochemical performance of this novel anode material was not comparable to that of the present first class anode materials, but, a novel group of anode material was really developed in this work, which might significantly lower the preparation cost of anode materials, being very favorable to the large scale production of anode materials.

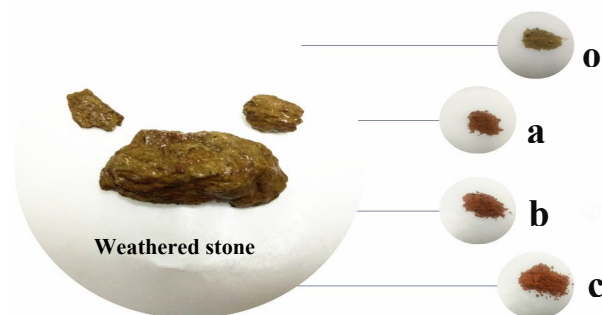
2. EXPERIMENTAL

2.1. Materials

Weathered stones are stones which can be easily crushed into small particles by hand, and all the weathered stones were obtained from Taihang Mountain of Hebei Province of China. All other chemical reagents were purchased from Tianjin Chemical Reagent Co. Ltd. All materials used in the electrochemical measurement, such as acetylene black, polyvinylidene fluoride, 1 M LiPF₆ electrolyte and the cell were all provided by the Tianjin Lianghuo S&T Developing Co. Ltd. All the chemicals were used as-received without any further purification.

2.2. Preparation of CWS anode materials

Briefly, the well cleaned and dried weathered stones were ground in an agate mortar for about 1 h to produce weathered stone powders. And then, these powders were pressed into pieces by a manual tablet machine. Lastly, above prepared pieces were put into a muffle furnace and calcined for 2 h at various temperatures under the air conditions. After cooling down to the room temperature, the resultant samples were ground in an agate mortar again leading to the formation of the products. The samples without calcination process was called as sample o, and these samples calcined at 400 °C, 600 °C and 800 °C were nominated as sample a, b and c, respectively. For comparison, the purchased pure SiO₂ was called as sample s. All the photos of the samples used in this work are shown in the Scheme 1. It can be seen that the weathered stone was yellow and brown, and after the calcination treatment, the color of the prepared samples turned into light brown.



Scheme 1. All samples employed in this work

2.3. Characterization

The crystal structures of the prepared samples were examined by using X-ray diffraction (Bruker AXS, D8 ADVANCE (Database version PDF-2004), Germany). The morphologies of all produced samples were viewed by scanning electron microscopy (HITACHI, SEM S-570) and transmission electron microscopy (HITACHI, TEM H-7650). Energy dispersive spectrometer (EDS, INCA Energy 350, England) was utilized to analyze the elemental components of the as-prepared samples. Fourier transform infrared spectrometry (FT-IR) measurements were conducted on a Hitachi FT-IR-8900 spectrometer (Japan) to detect the groups in the samples.

The electrochemical measurements of cyclic voltammetry (CV) and electrochemical impedance spectroscopy (EIS) were conducted on a CHI 660B electrochemical workstation (Shanghai Chenhua Apparatus, China) which was controlled by a personal computer. In the EIS measurements, the amplitude of the alternating current (AC) was 5 mV and the frequency ranges was from 100 kHz to 0.1 Hz. All the experiments were finished at room temperature.

The working electrodes were produced according to the following processes. First, the active material powders, acetylene black and polyvinylidene fluoride were mixed together at a weight ratio of 80:10:10 forming a mixture. And then, several drops of N-methyl pyrrolidone (NMP) were added into above mixture to form slurries after a careful agitation. Subsequently, the produced slurries were carefully smeared on a Cu foil using a glass piece, and then the resultant sample was dried in a vacuum drying oven at 120 °C for 6 h. The loading of all prepared working electrodes was approximately estimated to be around 1.5 mg cm⁻². The half-cells, i.e., the two-electrode cells mainly consisting of a lithium metal foil as the negative electrode, an electrolyte of 1 M LiPF₆, Celgard 2400 separator and the working electrode, were assembled in a high pure nitrogen-filled glove box (ZKX type of Nanjing NANDA instrument factory). It should be noted that the electrolyte was 1 M LiPF₆ and the mixed solvent contained dimethyl carbonate (DMC), ethylene carbonate (EC), ethyl methyl carbonate (EMC) and vinylene carbonate (VC). Evidently, metallic lithium foils were employed as both the reference and auxiliary electrodes. The apparatus of CT-3008W-5V20mA-S4 (Shenzhen Neware Electronics Co., Ltd. China) was used to complete the battery property measurement. The charge and discharge potential ranged from between 0.01 and 3 V at the current density of 100 mA g⁻¹.

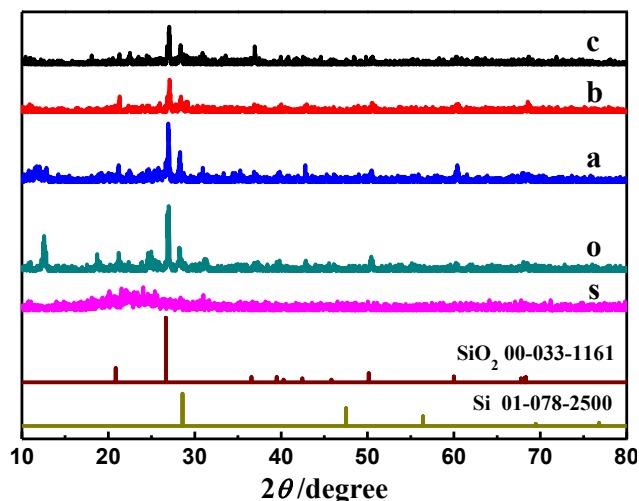


Figure 1. XRD patterns of all employed samples including the standard XRD patterns of SiO₂ and Si. Pattern s, o, a, b and c corresponded to sample s, o, a, b and c.

3. RESULTS AND DISCUSSION

3.1. XRD analysis

Fig.1 gives the XRD patterns for all the involved samples including the standard XRD patterns of SiO₂ and Si. For the pure SiO₂ (pattern s), a broad and weak diffraction peak appearing in the 18°-26° was displayed, agreeing well with the previous report regarding SiO₂ [18] which showed an amorphous characteristics. While for the pure weathered stone (pattern o), four diffraction peaks, positioned respectively at about 21°, 26°, 50° and 59°, were clearly exhibited, which effectively demonstrated that the main component of the weathered stone was SiO₂, basing on the comparison with the standard pattern of SiO₂. Interestingly, for all the calcined weathered stones, the typical diffraction peaks of SiO₂ were also clearly displayed, which effectively indicated that the main component of all CWS samples was SiO₂. Apparently, according to the comparison with the standard XRD pattern of Si, it was confirmed that no elementary Si was contained in all involved samples, further confirming that the main components of the samples were SiO₂. Meanwhile, the intensity of the diffraction peaks changed obviously with increasing the calcination temperature, which suggested that the crystallinities of the as-prepared samples were closely related to the calcination temperature. Close observation also revealed that less amounts of diffraction peaks were displayed in pattern b, which strongly evidenced that the purity of SiO₂ in sample b was higher when compared to other samples. For instance, the diffraction peak at 12.7° in pattern o disappeared totally in pattern b. Also, as the calcination temperature was up to 800°C, a small diffraction peak centered at about 18° came into being, which indicated that new substances were prepared in the synthesized samples. That is to say, the calcination temperature was a key role which not only affected the crystallinity of the prepared samples but also varied the component of the resultant samples.

Although the presence of other metal elements in the final samples was confirmed by the later EDS analysis, the evident diffraction peaks of metal oxides were not displayed in Fig.1. It indicated

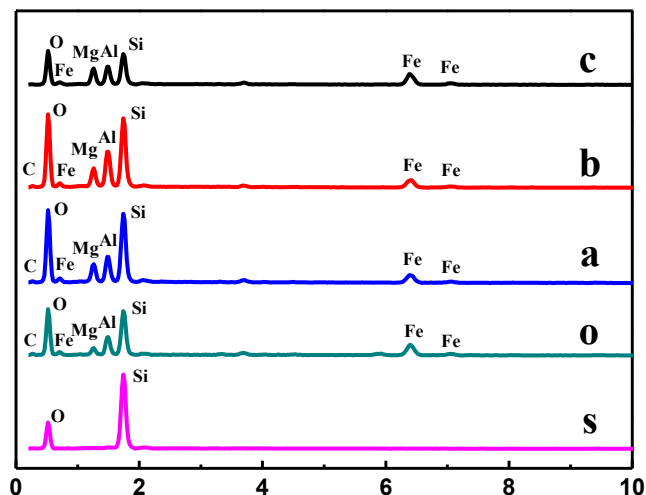


Figure 2. EDS patterns of all employed samples. Curve s, o, a, b and c corresponded to sample s, o, a, b and c.

that the amounts of metal oxides in the final samples were too lower to be detected, or suggested that these metal oxides were amorphous in nature. As far as we know, although some research works regarding the utilization of SiO₂ as anode materials for LIBs have been published recently [19,20], the report concerning the application of calcined weathered stone as anode material for LIBs has not been released so far, basing on our literature survey.

The elemental composition of the synthesized samples was also studied by EDS analysis, and the obtained results are illustrated in Fig.2. For the pure SiO₂, only elements of O and Si were detected (pattern s). While, for the pure weathered stone, the peaks corresponding to the elements of C, O, Mg, Al, Si and Fe were all clearly displayed, which indicated that the weathered stone was a mixture rather than a pure compound, and the main elements in weathered stone were Si, O and C. Apparently, the element atomic contents in the final products varied correspondingly with increasing the calcination temperature. For example, the atomic contents of Si, O and C in sample a were 20.26%, 54.05% and 5.10%. And the atomic contents of Si, O and C in sample b were 24.13%, 56.00% and 2.27%. And the atomic contents of Si, O and C in sample c were 22.23%, 59.76% and 0. That is to say, with increasing the calcination temperature, the content of carbon dropped sharply which was surely resulted from the burning of carbon. Meanwhile, the atomic content of O increased obviously which probably indicated that more amounts of metal oxides were formed in the final samples. For sample c, the atomic contents of Mg, Al and Fe were 4.25%, 4.25% and 4.54%, respectively. Therefore, it can be inferred that all the final products in this work were a mixture of oxides.

To further confirm the presence of functional groups in the final products, FTIR spectra of all the samples were presented in Fig.3. Apparently, all the FTIR spectra showed similar shape which demonstrated that identical functional groups were contained in all the samples. According to the previous work [21], the bands appearing at 1622 cm⁻¹ and 3362 cm⁻¹ were due to the presence of the

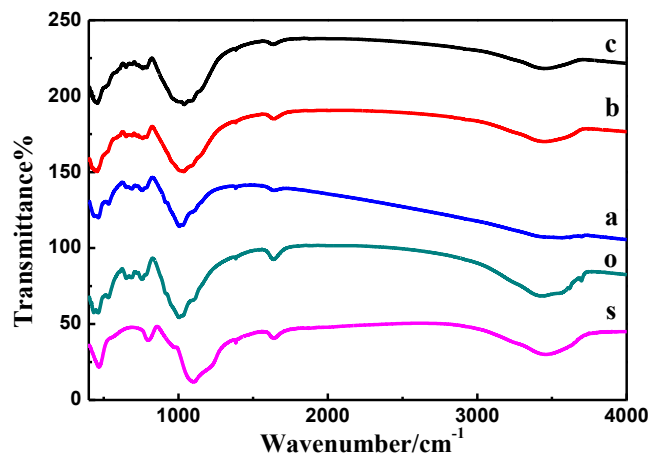


Figure 3. FTIR spectra for all employed samples. Curve s, o, a, b and c corresponded to sample s, o, a, b and c.

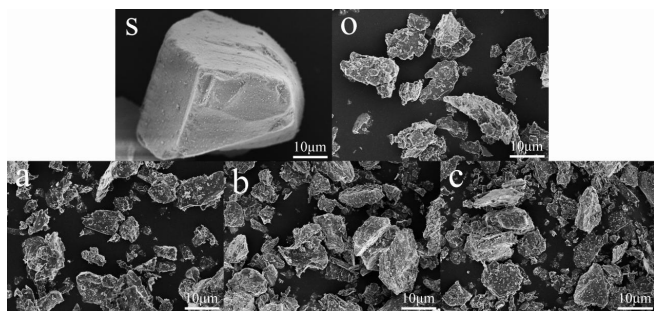


Figure 4. SEM images for all the used samples. Image s, o, a, b and c corresponded to sample s, o, a, b and c.

C-O and -OH groups, respectively, which was said to be originated from the adsorbed CO_2 and H_2O on the surface of the samples [21]. On the basis of the former report regarding SiO_2 [22], the band at 1105 cm^{-1} should be originated from the internal asymmetric stretching vibrations of Si-O-Si. And the smaller band at 959 cm^{-1} was from the symmetric stretching vibration of Si-OH. The bands positioned at 795 cm^{-1} and 473 cm^{-1} were attributed to the symmetric stretching vibration and the tetrahedral bending modes, respectively. Thus, the results of FTIR spectra further testified that the major component of all the samples was SiO_2 , which was consistent with the results of XRD patterns and EDS measurement.

3.2. Morphology characterization

SEM images of all the samples in this work are displayed in Fig.4. For the pure SiO_2 , huge particles with a diameter of more than $20\text{ }\mu\text{m}$ were seen clearly. While for other samples, relatively smaller particles with no regular crystal structure were exhibited. Apparently, no evident differences in both particle size and particle morphology were found for the weathered stone based samples. Thus, this result strongly implied that all the different properties exhibited by the samples should be attributed to their different components instead of the particle morphology or the particle size. Actually, after the calcination process, some substances disap-

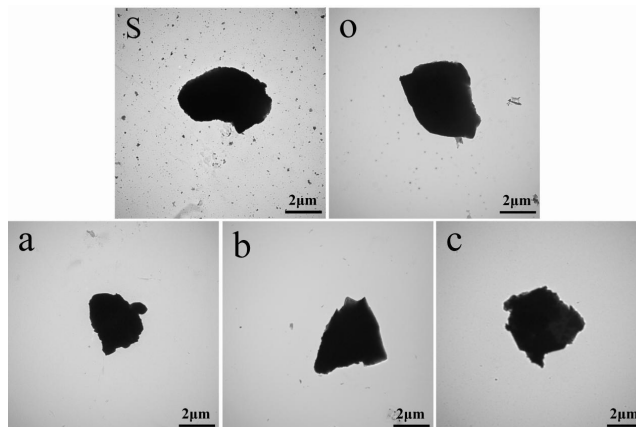


Figure 5. TEM images for all the used samples. Image s, o, a, b and c corresponded to sample s, o, a, b and c.

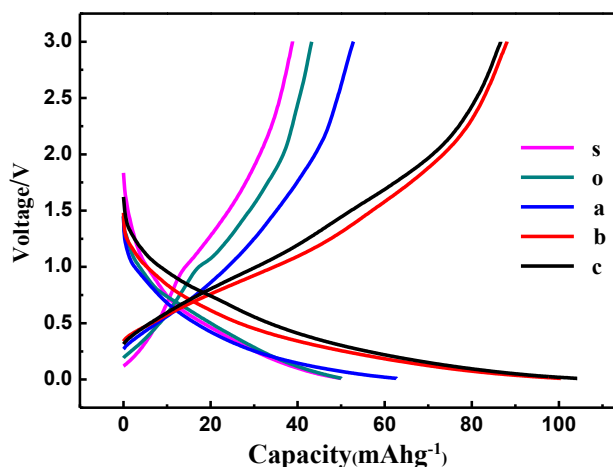


Figure 6. The initial charge-discharge profiles for all the samples which were recorded at a current density of 100 mA g^{-1} . Curve s, o, a, b and c corresponded to electrode s, o, a, b and c.

peared, as can be supported by the fact that some diffraction peaks existing in the XRD patterns of pure weathered stone (for example, the diffraction peak at 12.7° and 25° in pattern o) became invisible after the sintering process. That is to say, although no evident differences in morphology were found for the calcined weathered stones, the components of the resultant samples were rather different from each other.

TEM images for all the involved samples are provided in Fig.5. For all the samples, smaller particles with a diameter less than $5\text{ }\mu\text{m}$ were observed clearly, which strongly demonstrated that all the huge particles seen in Fig.4 were constructed by the smaller particles. Careful observation also indicated that all the smaller particles showed no evident crystal structure, which was consistent with the result in Fig.1 that the XRD patterns of all the samples showed relatively lower diffraction peaks, corresponding to a poor crystallinity of the samples. Also, it was clear that the edges of the pure weathered stone were straight, and after the calcination treatment,

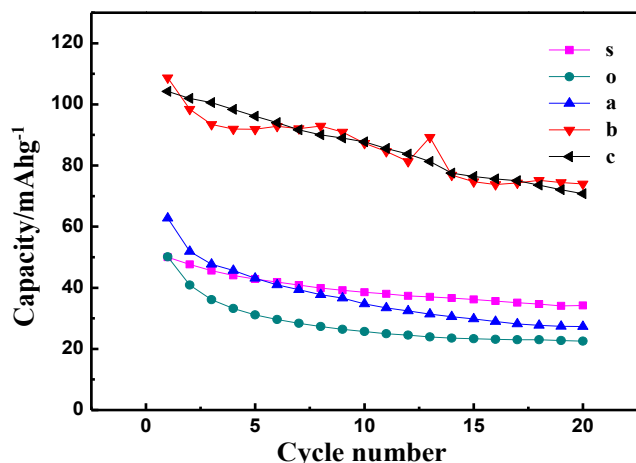


Figure 7. The cycling performances of all electrodes which were recorded at a current density of 100 mA g^{-1} . Curve s, o, a, b and c corresponded to electrode s, o, a, b and c.

the edges of the result particles became uneven. This consequence strongly verified that during the calcination process, some reactions took place which agreed well with the EDS analysis.

3.3. Electrochemical properties

The initial charge-discharge curves at a current density of 100 mA g^{-1} for all the samples are illustrated in Fig.6, in which the potential range is from 0.01V to 3 V. Obviously, sloped voltage plateaus are observed in both the discharging and charging process, which was very similar to that of hard carbon SiO_2 negative electrode[20]. The sloped discharge voltage line appearing in 1.00-0.10V should correspond to the reduction of Si^{4+} and the formation Li-Si-O. While, the sloped charge voltage line appearing in 0.10-1.90V should be originated from the oxidation reaction of anode material which was accompanied by the delithiation process leading to the formation of SiO_2 . Generally, the presence of a flat discharging or charging voltage plateau corresponded to a two-phase transformation [23]. The appearance of the sloped voltage plateau was probably attributed to the fact that all the samples were an oxide-containing mixture rather than a pure substance. Also, for all the samples, the charge-discharge curves showed similar shape which indicated that all the prepared electrodes had a similar charge-discharge mechanism. The initial discharge capacities for sample s, o, a, b and c were approximately evaluated to be 48, 50, 63, 104 and 102 mAh g^{-1} at the current density of 100 mA g^{-1} , respectively. In 2016, Choy's group [24] investigated the electrochemical performance of SiO_2 , and reported that the initial discharge capacity value of SiO_2 was up to 952 mAh g^{-1} at the current density of 30 mA g^{-1} . It should be noted that in their works, SiO_2 was prepared from tetraethylorthosilicate (TEOS) using a chemical method rather than from the weathered stone. In 2017, Gao's group [25] developed a simple method to fabricate the carbon conformal coating mesoporous hollow SiO_2 nanospheres ($\text{MHSiO}_2@\text{C}$), which delivered a high reversible capacity of $440.7 \text{ mA h g}^{-1}$ at a current density of 500 mA g^{-1} . Obviously, besides the large amounts of carbon coating, complicated structure of the prepared samples

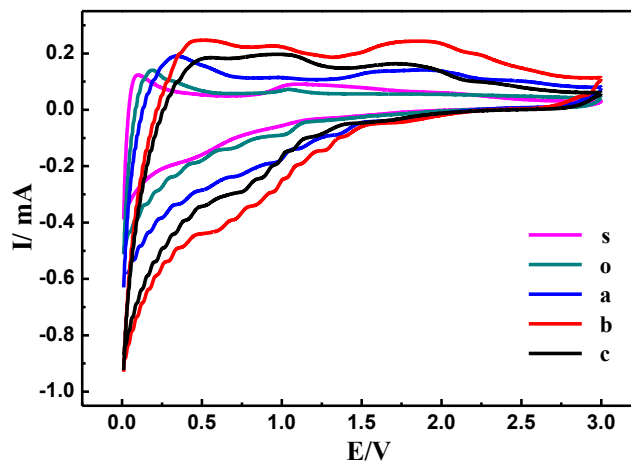


Figure 8. Cyclic voltammetry curves for all the prepared electrodes. Curve s, o, a, b and c corresponded to sample s, o, a, b and c. The scan rate was 1 mV s^{-1} .

was also involved in their works, which generally was not beneficial to the large scale production of anode materials. Although the discharge capacity delivered by the synthesized samples was lower than those of the currently reported SiO_2 -based composite anode materials, the work reported here was novel which was very meaningful to the large scale production of anode materials, due to the rather lower preparation cost and simple preparation process.

The cycling stability of an anode material is also a very important factor which can directly determine the serve life of a lithium ion battery. The cycling performance profiles of all samples are given in Fig.7. It can be seen clearly that in the whole testing period, sample b and c showed larger discharge capacity values when compared to other samples. For instance, after 20 cycles, the discharge capacities for the sample s, o, a, b and c was about 34, 22, 27, 74 and 71 mAh g^{-1} , which were equal to 68%, 44%, 43%, 69% and 68% of their initial discharge capacity value, respectively. Commonly, the relatively higher purity of an anode material is favorable to the electrochemical performance improvement of a lithium ion battery, basing on our previous report [26]. And the existence of carbon in the final sample is also advantageous to the enhancement of the electrical conductivity of anode materials due to the higher electrical conductivity of carbon itself, which can further promote the electrochemical behavior of a lithium ions battery [27]. Among these samples, sample b had a relatively higher purity as supported by the XRD analysis (Fig.1), and a proper amount of carbon was also contained in sample b (Fig.2). Therefore, sample b delivered a better electrochemical performance, as compared to other samples.

Cyclic voltammetry (CV) can be utilized directly to understand the insertion/extraction process of lithium ions in the prepared samples, and all the CV curves of all electrodes are shown in Fig.8. Evidently, some smaller redox peaks of CV are observed in the potential range, though no large oxidation and reduction peaks are seen for all the samples. In general, the anodic peak was accompanied by a delithiation process, and the cathodic peak was attributed to a lithiation process. Accordingly to the previous report, the peak

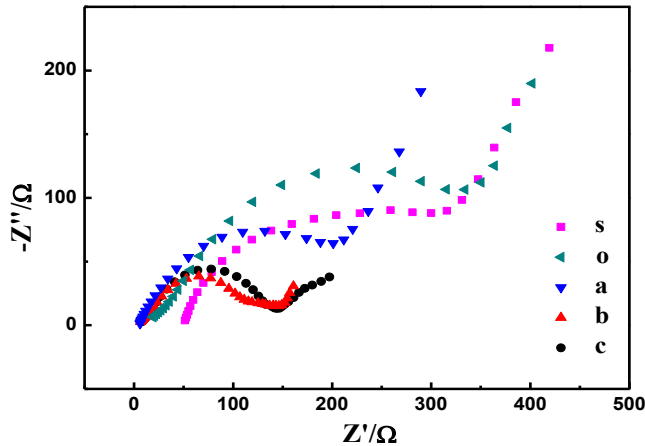
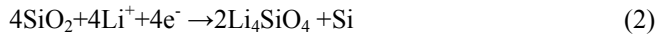


Figure 9. Nyquist plots of all the samples. Curve s, o, a, b and c corresponded to sample s, o, a, b and c.

near 0 V was closely related to the reversible alloy-dealloy reaction of silicon with Li ions [25], and the existence of redox peaks in the potential range of 0.9V-1.4 V were originated from the lithiation/delithiation process of SiO_2 . Namely, the charge-discharge process of lithium ions in SiO_2 mainly included the following reactions [20].



In this case, for the pure SiO_2 (curve s), except for the peak at 0V, there was a cathodic peak at about 0.45V and an anodic peak at 1.05V. While, for sample b and c, two broad anodic peaks (at 1.0V and 1.6V, respectively) appeared in the positive potential scan, which indicated that two delithiation processes were contained during the charging process. While, for sample a, only one broad and weak anodic peak was seen in the potential range of 1.6V-1.9V, which demonstrated that the mechanism of delithiation process in sample a was rather different from that of sample b and c. Unfortunately, for sample a, b and c, no evident cathodic peaks were found in the negative direction potential sweep, which strongly indicated that the intercalation/deintercalation process of lithium ions in the above samples was an irreversible process, which might lead to a poor cycling stability. Although sample o showed an anodic peak and a cathodic peak at the potential of about 1.0V, the peak area of curve o was the lowest one among all the samples, which could only correspond to a lower charge/discharge capacity value. Summarily, basing on the CV results shown in Fig.8 and the previous result [20] that larger particles of SiO_2 tended to form Li_4SiO_4 and Si, it can be concluded that reaction (2) and (3) should be involved in the intercalation/deintercalation process of lithium ions for all the resultant samples. Commonly, the peak area of a CV curve was directly proportional to the amount of electric charges consumed in an electrochemical reaction [28]. Accordingly, for the CV curve measured on a half-cell of LIBs, the peak area of CV curve was directly proportional to the amounts of lithium ions

transferred in the lithiation/delithiation process. Thus, it was clear that the whole peak area of electrode b was the largest one among all the samples. Consequently, electrode b delivered the largest discharge capacity value among all the prepared electrodes, which was consistent with the results shown in Fig.6 and Fig.7.

As a traditional research method in electrochemistry, electrochemical impedance spectroscopy (EIS) has been widely employed to examine the behavior of a lithium ion half-cell. Although there are many kinds of curves in EIS, Nyquist plots as one typical kind of curves are generally used in studying the electrochemical performance of Li half-cells mainly due to its simplicity and intuitiveness. It should be emphasized that all the Nyquist plots in Fig.9 were recorded after 20 cycles and all the curves were measured at their open circuit potentials. Apparently, the shape of all Nyquist plots shown in Fig.9 was very similar to that of the previously published Nyquist plot regarding a lithium ion half-cell [23, 29], which also indicated that the mechanism of the lithiation/delithiation process in the employed samples was close to that of the previously published work. Generally, the intercept at the Z_{real} axis (here was Z') was stemmed from the total ohmic resistance (R_o). And the depressed semicircle displayed in the high-to-middle frequency range was commonly resulted from a parallel circuit that contained a capacitive element and a resistor unit, and the diameter value of this depressed semicircle was approximately equal to the value of the charge transfer resistance (R_{ct}). And the oblique line in the lower frequency region called as the Warburg impedance was mainly attributed to the lithium-ion diffusion in the electrode materials [29]. In above parameters, R_{ct} is the most widely used parameter by which the kinetics of a lithium ion-based electrode reaction can be compared directly [29]. Ordinarily, a faster lithium insertion/extraction kinetics corresponded to a smaller value of R_{ct} . Basing on our previous work concerning LIBs [30], the values of R_{ct} for electrode s, o, a, b and c, which can be roughly evaluated from the diameter of the depressed semicircle, were 350 Ω , 400 Ω , 245 Ω , 150 Ω and 175 Ω , respectively. Thus, electrode b showed the smallest value of R_{ct} among all the samples which indicated that sample b had the fastest lithium insertion/extraction kinetics among all the resultant samples. This result should be well responsible for the fact that sample b had the best electrochemical performance among all the samples.

On the basis of the former report, the Li-ion diffusion coefficient in an anode material can be estimated by the following formula [31].

$$D_{\text{Li}} = \frac{(RT)^2}{2An^2F^2C_{\text{Li}}\sigma^2} \quad (4)$$

In this formula, A represented the surface area of the working electrode, n the number of electrons transferred in an electrochemical reaction, C_{Li} was the concentration of lithium ion in the solid anode material, and R, T and F had their conventional scientific meanings. σ , named as Warburg factor, was a parameter which can only be obtained from the following equation [32].

$$Z_{re} = R_s + R_{ct} + \sigma \omega^{-1/2} \quad (5)$$

In above equation, Z_{re} (here is Z') is the real part of the impedance; R_s the resistance of electrolyte; R_{ct} the charge transfer re-

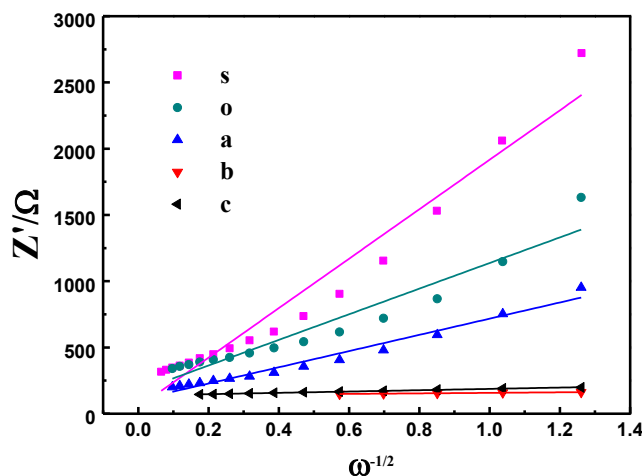


Figure 10. The curves of Z' against the reciprocal of square root of ω ($\omega^{-1/2}$). Curve s, o, a, b and c corresponded to sample s, o, a, b and c.

distance and ω is the angular frequency in the low frequency region. The typical curves of Z_{re} against $\omega^{-1/2}$ for these five samples are illustrated in Fig.10, thus, the values of σ can be obtained directly from the slope of these plots. Evidently, the exact value of D_{Li} cannot be estimated directly since the value of both n and C_{Li} were unknown to us. But the values of D_{Li} for these five samples could be compared approximately when the value of σ was confirmed, supposing that the values of n and C_{Li} were identical in all employed samples. Apparently, a smaller value of σ corresponded to a larger value of D_{Li} . Therefore, the lithium diffusion coefficients of D_{Li} for these electrodes were in the following decreasing order, i.e., electrode $b > c > a > o > s$. The result strongly indicated that it was easier for lithium ions to diffuse in sample b when compared to other samples, which accorded well with the fact that sample b had the best electrochemical performance among all the samples.

4. CONCLUSIONS

For the first time, a novel finding, that the calcined weathered stones can be employed as anode materials for LIBs, is reported in this work, which is very helpful to the large scale production of anode materials for LIBs mainly due to the valueless raw materials and the rather simple preparation process. XRD and EDS analysis revealed that the main component of both the calcined weathered stone and the pure weathered stone was SiO_2 . SEM and TEM images indicated that no evident differences in the morphology were found for all the samples, which effectively testified that the differences in electrochemical performances of all the samples should be mainly attributed to their different components rather than the particle morphology and particle size. Also, it was demonstrated that the calcination temperature played a key role in influencing the electrochemical behavior of the produced samples, and $600^\circ C$ -calcined weathered stone (sample b) showed the best electrochemical performance among all the prepared samples, namely, the discharge capacity of sample b was close to 70 mAh g^{-1} after 20 cycles at a current density of 100 mA g^{-1} . Although the electrochemical

performance exhibited by the calcined weathered stone was not superior to that of the currently studied SiO_2 -based anode materials, this novel finding has opened a new field regarding the anode materials of LIBs, which was very beneficial to the further commercialization of LIBs.

5. ACKNOWLEDGMENTS

This work was financially supported by the National Natural Science Foundation of China (No. 21173066 and 21403052), Natural Science Foundation of Hebei Province of China (No. B2011205014, B2015205150 and 2015205227), Z.G. acknowledges the support from the U.S. National Science Foundation (Nanoscale Interdisciplinary Research Team and Materials Processing and Manufacturing) under Grant CMMI 10-30755.

REFERENCES

- [1] L. Croguennec, M. Rosa Palacin, *Journal of the American Chemical Society*, 137, 3140 (2015).
- [2] X. Lu, L. Gu, Y.-S. Hu, H.-C. Chiu, H. Li, G. P. Demopoulos, L. Chen, *Journal of the American Chemical Society*, 137, 1581 (2015).
- [3] Y. Wang, X. Wen, J. Chen, S. Wang, *Journal of Power Sources*, 281, 285 (2015).
- [4] H. Tian, X. Tan, F. Xin, C. Wang, W. Han, *Nano Energy*, 11, 490 (2015).
- [5] H. Shobukawa, J. Alvarado, Y. Yang, Y. S. Meng, *Journal of Power Sources*, 359, 173 (2017) 173-181.
- [6] C. Liu, X. Liu, J. Tan, Q. Wang, H. Wen, C. Zhang, *Journal of Power Sources*, 342, 157 (2017).
- [7] K. Ding, P. Wang, J. Zhao, Y. Li, Y. Chen, Y. Zhang, B. Wei, Y. Sun, J. Pan, *International Journal of Hydrogen Energy*, 42, 9766 (2017).
- [8] S. Cho, H. Y. Jang, I. Jung, L. Liu, S. Park, *Journal of Power Sources*, 362, 270 (2017).
- [9] I. Meschini, F. Nobili, M. Mancini, R. Marassi, R. Tossici, A. Savoini, M. L. Focarete, F. Croce, *Journal of Power Sources*, 226, 241 (2013).
- [10] Y. Deng, C. Fang, G. Chen, *Journal of Power Sources*, 304, 81 (2016).
- [11] Z. Li, X.-Y. Yu, U. Paik, *Journal of Power Sources*, 310, 41 (2016).
- [12] T. V. Thi, A. K. Rai, J. Gim, J. Kim, *Journal of Power Sources*, 292, 23 (2015).
- [13] K. Ding, J. Zhao, M. Zhao, Y. Chen, Y. Zhao, J. Zhou, *International Journal of Electrochemical Science*, 11, 2513 (2016).
- [14] K. Ding, J. Zhao, J. Zhou, Y. Zhao, Y. Chen, Y. Zhang, B. Wei, L. Wang, X. He, *International Journal of Electrochemical Science*, 11, 446 (2016).
- [15] K. Ding, J. Zhao, J. Zhou, Y. Zhao, Y. Chen, L. Liu, L. Wang, X. He, Z. Guo, *Materials Chemistry and Physics*, 177, 31 (2016).
- [16] S. Zhang, P. Zhang, A. Xie, S. Li, F. Huang, Yuhua Shen, *Electrochimica Acta*, 212, 912 (2016).
- [17] S.-W. Kim, D. T. Ngo, J. Heo, C.-N. Park, C.-J. Park, *Electro-*

- chimica Acta, 238, 319 (2017).
- [18]H. Wang, X. Li, X. Zhuang, B. Cheng, W. Wang, W. Kang, L. Shi, H. Li, Journal of Power Sources, 340, 201 (2017).
- [19] X. Liu, Y. Chen, H. Liu, Z.-Q. Liu, Journal of Materials Science & Technology, 33, 239 (2017).
- [20]B. Guo, J. Shu, Z. Wang, H. Yang, L. Shi, Y. Liu, L. Chen, Electrochemistry Communications, 10, 1876 (2008).
- [21]K. Ding, J. Zhao, J. Zhou, Y. Zhao, Y. Chen¹, Y. Zhang, B. Wei, L. Wang, X. He, International Journal of Electrochemical Science, 11, 446 (2016).
- [22]J. Meng, Y. Cao, Y. Suo, Y. Liu, J. Zhang, X. Zheng, Electrochimica Acta, 176, 1001 (2015).
- [23]K. Ding, H. Gu, C. Zheng, L. Liu, L. Liu, X. Yan, Z. Guo, Electrochimica Acta, 146, 585 (2014).
- [24]D.W. Choi, K.-L. Choy, Electrochimica Acta, 218, 47 (2016).
- [25]W. An, J. Fu, J. Su, L. Wang, X. Peng, K. Wu, Q. Chen, Y. Bi, B. Gao, X. Zhang, Journal of Power Sources, 345, 227 (2017).
- [26]K. Ding, J. Zhao, Y. Sun, Y. Chen, B. Wei, Y. Zhang, J. Pan, Ceramics International, 42, 19187 (2016).
- [27]K. Ding, Y. Zhao, L. Liu, Y. Li, L. Liu, L. Wang, X. He, Zhanhu Guo, Electrochimica Acta, 176, 240 (2015).
- [28]K. Ding, T. Okajima, T. Ohsaka, Electrochemistry, 75, 35 (2007).
- [29]D. Cui, Z. Zheng, X. Peng, T. Li, T. Sun, L. Yuan, Journal of Power Sources, 362, 20 (2017).
- [30]G.-Q. Zhang, W. Li, H. Yang, Y. Wang, S. B. Rapole, Y. Cao, C. Zheng, K. Ding, Z. Guo, Journal of New Materials for Electrochemical Systems, 16, 25 (2013).
- [31]A.Y. Shenouda, H.K. Liu, Journal of Power Sources, 185, 1386 (2008).
- [32]T.-F. Yi, H. Liu, Y.-R. Zhu, L.-J. Jiang, Y. Xie, R.-S. Zhu, Journal of Power Sources, 215, 258 (2012).